Acta Crystallographica Section D
Biological Crystallography
ISSN 0907-4449

Decoration of microtubules in solution by the kinesin-14, Ncd

Rex P. Hjelm,[a]* Deborah Bennett Stone,[b] Robert J. Fletterick[b] and Robert A. Mendelson[b]†

[a]Los Alamos Neutron Science Center, Los Alamos National Laboratory, Los Alamos, NM 87545, USA, and [b]Department of Biochemistry and Biophysics, University of California, San Francisco, CA 95128-2517, USA

† Deceased.

Correspondence e-mail: hjelm@lanl.gov

Received 19 April 2010
Accepted 3 June 2010

The kinesin-14, Ncd, is a cellular motor involved in microtubule spindle assembly and contraction during mitosis and meiosis. Like other members of the kinesin superfamily, Ncd consists of two motor heads connected by a linker and a long cargo-carrying stalk. The motor heads hydrolyze ATP to ADP to provide the power stroke that moves them and the cargo along the microtubule. Whereas conventional kinesins move processively along the sense of the microtubule right-handed helix, Ncd moves in the opposite direction, apparently using a different motive mechanism. According to the current model, the microtubule-binding state of Ncd is bound by one head and then released during the motive cycle. This is distinguished from the binding states of conventional kinesins, in which the motor heads are always bound in the motive cycle with alternating one-head and two-head binding. The objective was to determine the extent of binding, the binding states of Ncd in the presence of an ATP analogue, AMPPNP, and whether the binding is cooperative. Small-angle neutron scattering (SANS) of microtubules decorated with a deuterated Ncd construct, Ncd281, in solution containing 42% D_2O was used. These conditions render the microtubule 'invisible' to SANS, while amplifying the SANS from the Ncd constructs. In the presence of AMPPNP, 75% of Ncd281 was not bound. The remainder was bound cooperatively by one of its motor heads to the microtubule.

1. Introduction

Ncd (kinesin-14) is a cellular motor that is responsible for chromosome movement by spindle fiber contraction during mitotic and meiotic anaphase and also participates in spindle assembly and growth (Fink *et al.*, 2009). Like other members of the kinesin family, Ncd consists of two motor heads connected by a linker and a long cargo-carrying stalk (Sablin, 2000). In each kinesin the motor heads use the hydrolysis of ATP to ADP to move along cytoskeleton elements, microtubules, providing essential cellular functions (Vale, 2003). Ncd moves in the negative direction, against the sense of the right-handed helix of the tubulin dimers that make up the microtubule. Thus, it differs from conventional kinesin, which moves in the opposite direction.

Conventional kinesins move by a processive head-over-head motion (Sablin & Fletterick, 2004) involving alternating one-head and two-head binding states. The one-head binding state results when one motor head without nucleotide is bound to the microtubule and the other with ADP is unbound and distal to the microtubule. The two-head binding state occurs when the bound head binds ATP, swinging its partner, which has released ADP, to the next tubulin dimer, where it binds

producing the two-head binding state. Ncd, on the other hand, appears to be nonprocessive. Cryo-TEM studies indicate that Ncd alternates between being in the one-head binding state in the presence of ATP or with no nucleotide and free in the presence of ADP (Wendt *et al.*, 2002; Endres *et al.*, 2006).

TEM studies of microtubule decoration by conventional kinesin (Vilfan *et al.*, 2001), Ncd (Wendt *et al.*, 2002) and the Ncd-like heterodimer VIK1/KER3 (Allingham *et al.*, 2007) show large contiguous decorated regions of the microtubules, leaving other regions of the microtubule undecorated. Either one-head or two-head binding states could be present in each of the cooperative binding regions, but the two states, if present, must exist in separate cooperative binding regions (Vilfan *et al.*, 2001). Cooperative binding may have implications for the motive mechanism of Ncd (Furuta & Toyoshima, 2008; Furuta *et al.*, 2008) and for Ncd function in spindle fiber contraction.

Our objective was to perform solution studies of the binding characteristics of Ncd and determine the extent of binding and whether one-headed cooperative binding with microtubules occurs in solution in the presence of ATP, as observed in the previous TEM studies. Although a structure for bound Ncd has been proposed through TEM studies (Wendt *et al.*, 2002; Endres *et al.*, 2006), such studies tend to focus on one aspect of the binding. Other states, including unbound states, may exist that could relate to understanding the motive mechanism of Ncd and influence the results and conclusions from biochemical studies (*e.g.* Foster & Gilbert, 2000; Allingham *et al.*, 2007).

We used small-angle neutron scattering (SANS) of Ncd-decorated microtubules in solution to observe the radial density function of the motor heads of an Ncd construct, Ncd281, decorating microtubules in the presence of an ATP analogue, 5-adenylylimidodiphosphate (AMPPNP). Ncd281 contains both motor heads as a dimer with a connecting linker region. The one-head and two-head cooperative and random binding states of Ncd will have distinctive SANS signatures. In our studies, nondeuterated microtubules in 42% D_2O were decorated with Ncd281 with 94% deuteration. This procedure amplified the signal from the Ncd construct, while rendering the microtubule nearly 'invisible' to SANS. In the presence of AMPPNP the prevalent state for Ncd281 was with one motor head of the dimer bound to the microtubule. The binding was found to be cooperative.

2. Materials and methods

2.1. Expression and purification of motor proteins

Drosophila Ncd281 motor-domain dimers (Glu281–Lys700) were prepared as described previously (Stone *et al.*, 1999; Fujiwara *et al.*, 1995) using deuterated medium for cell growth (Stone *et al.*, 1998).

2.2. Preparation of motor protein–microtubule complexes

Tubulin was prepared from bovine (veal) brain tissue using the procedure of Diaz *et al.* (1998). Aliquots of taxol-stabilized microtubules were mixed with a twofold to threefold molar excess of motor protein in buffer containing 42% D_2O, as described by Marx *et al.* (1998), with apyrase (1–2 units ml^{-1}) and 1 m*M* AMPPNP. Excess motor protein was removed by pelleting the microtubule–motor protein complex at room temperature through a 60% glycerol cushion in buffer as above with the addition of 100–200 m*M* NaCl. The pelleted microtubule–motor protein complexes were resuspended in microtubule-resuspension solution consisting of 100 m*M* NaCl with AMPPNP.

2.3. Protein characterization

Protein concentrations were determined by biuret (Gill & von Hippel, 1989) or spectrophotometrically (White, 1982). After SANS measurements the sample was run on three separate 7.5% Bio-Rad gels at different concentrations or loadings. The dried gels were scanned with a Kodak EDAS290 densitometer using one-dimensional analysis to determine the area of each band. The ratio of Ncd heads to tubulin monomer was determined from area of the Ncd band divided by the area of the tubulin band.

2.4. Small-angle neutron scattering

The SANS was measured using the time-of-flight Low-Q Diffractometer (LQD) at the Manuel Lujan Neutron Scattering Center at Los Alamos National Laboratory. The scattering data were reduced differential scattering cross-section per unit solid angle, as described previously (Hjelm, 1988; Seeger & Hjelm, 1991), and were placed on an absolute scale of per tubulin dimer, $d\sigma_T(Q)/\delta\Omega$ (cm^2). Here, Q ($Å^{-1}$) is the momentum transfer, which is equal to $Q = 4\pi/\lambda \sin\theta$, where λ (Å) is the neutron wavelength and 2θ is the scattering angle.

3. Theory

The theory of scattering from rod-like structures describes the intensity as a sum of squared cylindrical Bessel functions, J_n (Hjelm, 1985). For the low-Q values accessed in a SANS measurement only J_0, around the zero-order layer line contributes to the scattering (Andreu *et al.*, 1992).

In the case of cooperative binding, sections of microtubules are uniformly decorated in either one-headed or two-headed binding states or are bare. Each decorated or undecorated microtubule section is made up of an identical repeating motif of up of N units in the helical repeat, each of which has n_0 ($Å^{-1}$) repeats per unit length. If we use the approximation, valid for the vignette of the SANS measurement, that each type of uniform section is long enough to be considered infinite, then the scattering is given by the square of the zero-order Hankel transform of the rod scattering-length density, $\rho(r, z, \xi)$, averaged about the azimuth, ξ, and projected down the rod length, z, to give the radial scattering-length density, $a_0(r)$; thus,

$$\frac{d\sigma(Q)}{d\Omega} = \frac{\pi}{Qn_0}\left|\int r a_0(r) J_0(Qr)\, dr\right|^2, \qquad (1)$$

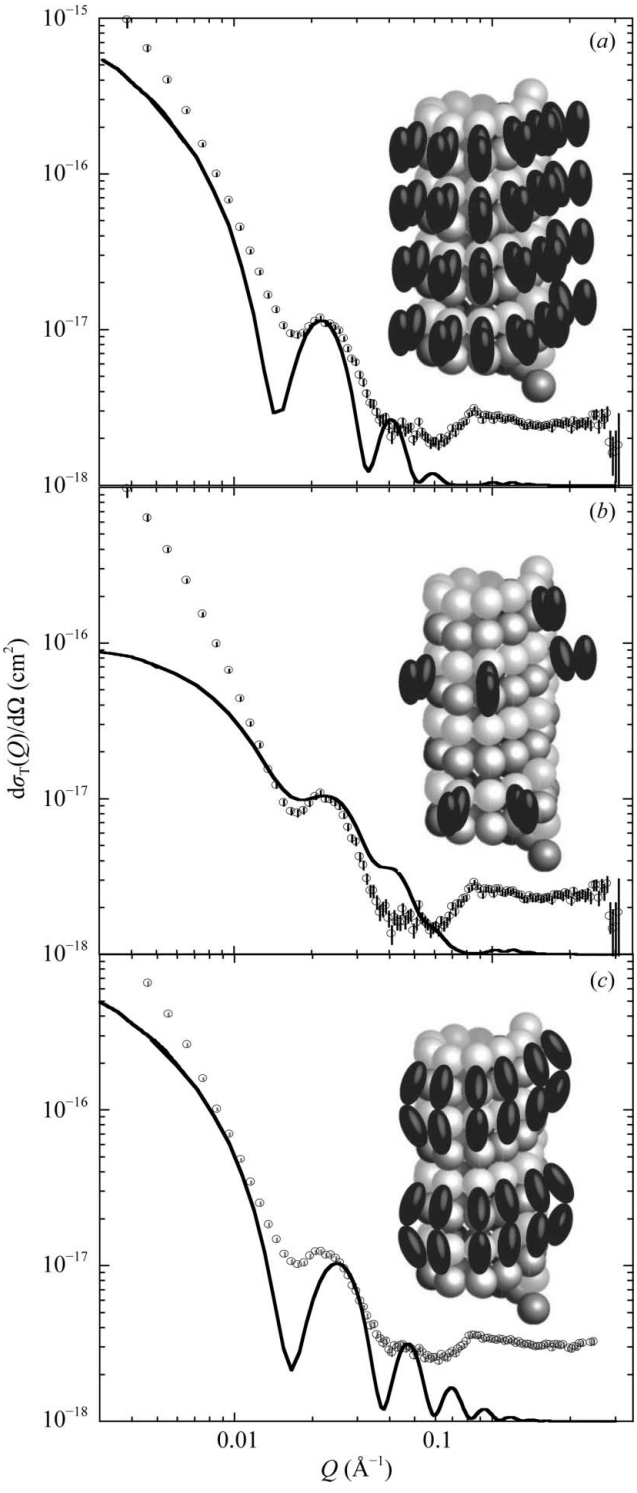

Figure 1
SANS differential cross-sections of Ncd281 microtubules in $f_D = 0.42$ D_2O with AMPPNP and comparison with models. Ncd281 data are shown as circles. Total particle densities for Ncd281: $N = 3.92 \times 10^{16}$ cm^{-3} motor dimers; $N = 5.89 \times 10^{16}$ cm^{-3} tubulin dimers. Scattering intensity calculated for models: (*a*) one-head cooperative binding; (*b*) one-head random binding with an average of approximately one motor per helical turn; (*c*) two-head cooperative binding. In each of the cooperative binding models sections of decorated microtubules coexist with sections of undecorated microtubules. Model parameters are given in Table 2. All values are per tubulin dimer, $d\sigma_T(Q)/d\Omega$ (cm^2), scaled and corrected for the fraction of unbound Ncd as described in the text.

normalized to the number density of repeating molecular units (cm^{-3}). With the assumption of infinite section length, then the total scatter from a collection of uniformly decorated and bare rods is the sum of the scattering intensity from each.

For the case of random binding of Ncd281, we assume that the probability of a binding site being occupied is independent of the occupancy of its neighbours, and then otherwise, with the same assumptions used in (1), the scatter is given by (Hjelm, 1985),

$$\frac{d\sigma(Q)}{d\Omega} = \frac{\pi}{Qn}\left\langle \overline{M'(Q)}^2 \right\rangle + \frac{4\pi^2 c}{n}\left[\left\langle \overline{M(Q)^2} \right\rangle - \left\langle \overline{M(Q)}^2 \right\rangle\right], \quad (2a)$$

$$\left\langle \overline{M'(Q)}^2 \right\rangle = \left[\sum_i f_i \int r a_{0i}(r) J_0(Qr)\, dr\right]^2, \quad (2b)$$

$$\left\langle \overline{M(Q)}^2 \right\rangle = \left\langle \left[\sum_i f_i \int r a_{0i}(r) J_0(Q_k r)\, dr\right]^2 \mathrm{sinc}^2\left(\frac{Q_l c}{2}\right)\right\rangle, \quad (2c)$$

$$\left\langle \overline{M(Q)^2} \right\rangle = \left\langle \sum_i f_i \left[\int r a_{0i}(r) J_0(Q_k r)\, dr\right]^2 \mathrm{sinc}^2\left(\frac{Q_l c}{2}\right)\right\rangle. \quad (2d)$$

Here, $\mathrm{sinc}^2 x = \sin^2 x/x^2$; Q_k and Q_l are the components of vector **Q** perpendicular to and along the rod axis, respectively. The angle brackets indicate a spherical average. (2*c*) and (2*d*) give the intensity that is not confined to the layer line.

The sums in (2) are over the occurrence of different motifs *i*, each of which occurs with probability f_i. Here, we defined the motif as one helical repeat of the microtubule containing N tubulin dimers and n (Å^{-1}) = n_0 is the number of variable motifs per unit length. Of the two possible binding states, we found that the predominant one in the presence of AMPPNP is the one-head binding mode. Thus, there are then $N + 1$ distinct motifs in the decorated microtubule differing by the number of decorated tubulin dimers that are present in a microtubule helical repeat, n, and we may adopt a simple binomial distribution for $f_i = f_n$ given the probability P that a tubulin dimer is decorated and $Q = 1 - P$ that it is not,

$$f_n = \frac{N!}{n!(N-n)!} P^n Q^{N-n}. \quad (3)$$

We used $N = 12$, which is consistent with the TEM and small-angle X-ray (SAXS) data of Andreu *et al.* (1992) and Diaz *et al.* (1998) that the majority of taxol-stabilized microtubules are in a 12/3 helical structure. Out SANS data of taxol-stabilized microtubules confirm this (Fletterick & Mendelson, 2010).

Scattering simulations of microtubules decorated with either Ncd281 were performed using a program written for this purpose, *MTScat*. *MTScat* uses coordinates from the Protein Data Bank (PDB) to construct the radial scattering-length density function, $a_0(r)$ (1 and 2), as a series of discrete cylindrical shells, each δr thick. The shell thickness was chosen in accordance with the Shannon Theorem (Bracewell, 1978) as $\delta r = (2Q_{max})^{-1}$, where Q_{max} is the largest Q value used in the transforms (1 and 2). The $a_0(r)$ included the scattering-length density, ρ_s, of solvent included in each shell to compute the radial scattering-length density functions as

$$a_0(r) = \frac{\sum_j b_j + \left(V_{\rm shell} - \sum_j V_j\right)\rho_{\rm s}}{V_{\rm shell}} - \rho_{\rm s}. \quad (4)$$

The scattering-length densities in (4) were calculated for each amino-acid residue using the total scattering lengths, b_j, and volumes, V_j, given by Jacrot & Zaccai (1981) and assuming that a fraction (0.8) is exchangeable hydrogen.

Decorated microtubules were assumed to have 12/3 helical microtubule symmetry. We used PDB file 1tub for the tubulin dimer coordinates (Nogales *et al.*, 1998) and the 12/3 helix coordinates set using *UCSF Chimera* (Pettersen *et al.*, 2004). We used the coordinates of the mutant construct Ncd600K (Yun *et al.*, 2003; PDB entry 1n6m), corresponding to the microtubule-bound ATP state of Ncd (Endres *et al.*, 2006), for the for one-head bound state, which was docked to the tubulin dimer by hand using *UCSF Chimera*. We modelled the two-head binding state using the coordinates of the Ncd dimer determined by X-ray crystallography (Sablin *et al.*, 1998; PDB entry 2ncd) docked onto the tubulin dimer using the data of Kikkawa *et al.* (2001) (provided by E. Sablin), but with the distal head removed. The motor packing on the microtubule used for one-head and two-head cooperative binding is shown schematically in Figs. 1(*a*) and 1(*c*), respectively, and that for random one-head binding is shown in Fig. 1(*b*). The simulated scatter was convoluted with the LQD instrument resolution function (Hjelm, 1988) and a constant incoherent background was added. The models took into account the fraction of microtubule that is decorated, $\psi = P$, the fraction of Ncd281 bound, φ, the probability, p, of one head binding and the molar ratio of Ncd281 to tubulin dimer in the solution, $d_{\rm D}$. These parameters are interrelated by the condition

$$\left(\frac{1+p}{2d_{\rm D}}\right)\frac{\psi}{\varphi} = 1. \quad (5)$$

4. Results

The concentration of Ncd281 dimer assayed by PAGE in the solution with tubulin dimer was not sufficient to decorate all of the microtubules, as $d_{\rm D} = d_{\rm M}/2$ was less than the expected value $d_{\rm D} = 1$ for complete decoration (Table 1), even though the initial mixture contained a twofold to threefold excess of motor protein.

SANS showed distinct evidence of microtubule decoration (Fig. 1), as the hallmarks of rod-like scattering were clearly seen. This is evident from comparison with the calculated SANS intensities in Figs. 1 and 2. Fig. 2 shows $d\sigma_{\rm T}(Q)/d\Omega$ calculated for 12/3 helical microtubules in $f_{\rm D} = 0.42$ D_2O and examples of deuterated Ncd281 in one-head and two-head binding states, assuming complete microtubule decoration. Fig. 2 shows that the one-head and two-head binding states can be distinguished, as the positions and intensities of the first-order J_0 peaks (1) indicate the decorated microtubule radius. The position of the peak at $Q \simeq 0.022$ Å^{-1} observed in the SANS data (Fig. 1) is exactly that anticipated for the one-head binding case (Fig. 2). An estimate of the incoherent background at $\sim 10^{-18}$ cm^2 shows the limit of detection of the scattering features and that the signal from microtubules would be at least two orders of magnitude smaller than from that from fully decorated microtubules.

Table 1
Solution concentrations and Ncd281 heads per tubulin dimer determined from PAGE.

Motor head concentration (μM)	Tubulin dimer concentration (μM)	Total Ncd heads per tubulin dimer $d_{\rm M}$
130	98	1.33 ± 0.22

A comparison of SANS absolute intensity (Fig. 1) with the calculated SANS (Fig. 2) shows that the data are significantly less than anticipated for complete binding of the microtubule. From this observation and the values in Table 1 both φ and ψ were considerably less than one.

The free Ncd construct will make a significant contribution to the SANS data and had to be taken into account in our calculations. To estimate φ, we subtracted the scattering signal expected for different amounts of free dimer from the normalized data for the peak value at $Q = 0.022$ Å^{-1} and the intensities co-plotted with the model intensities scaled for various values of φ. The value of φ was the point at which the

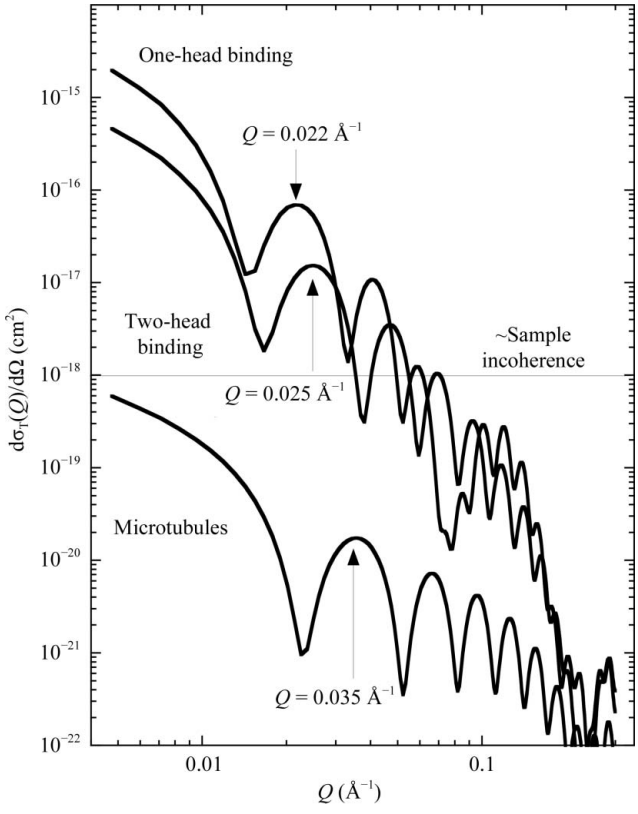

Figure 2
Model calculations of microtubules and microtubules decorated with deuterated Ncd281 in $f_{\rm D} = 0.42$ D_2O. SANS for models, including instrument resolution smearing, are shown for undecorated 12/3 helical microtubules, microtubules decorated in the one-head binding state and microtubules decorated in the two-head binding state. All values are per tubulin dimer, $d\sigma_{\rm T}(Q)/d\Omega$ (cm^2).

Table 2
Model parameters for Ncd281-decorated microtubules in the presence of nucleotide.

	p	φ	ψ	Δm_0 (cm^2 Å^{-1})	R_c (Å)	n (Å^{-1})	Tubulin-bound motor head R_{min} (Å)	Tubulin-bound motor head R_{max} (Å)	Unbound motor head R_{min} (Å)	Unbound motor head R_{max} (Å)
One-head cooperative binding	1.0	0.25	0.17	3.8×10^{-18}	171	0.15	121	189	159	211
One-head random binding	1.0	0.13	0.09	—	—	0.15	121	189	159	211
Two-head cooperative binding	0	0.46	0.61	8.5×10^{-19}	150	0.15	120	189	—	—
Microtubule parameters	—	—	—	9.0×10^{-22}	104	0.15	75	138	—	—

two lines intersected. The scatter attributed to the decorated microtubule in the sample was calculated by subtraction of the $1 - \varphi$ free Ncd281 component using SANS data for deuterated Ncd281 (Fletterick & Mendelson, 2010). The data in Fig. 1 have been corrected for the presence of free Ncd281 for each of the models; thus, it only represents the signal from the deuterated Ncd-decorated microtubules. The data above Q = 0.07 Å^{-1} are likely to be an artifact of subtracting the signal from the free Ncd281.

The model for one-head cooperative binding (Fig. 1*a*) coexisting with undecorated microtubules, as given in Table 1, reproduces well the position and amplitude of the peak at 0.022 Å^{-1}. However, the model gave a lower intensity than the data at the lowest Q values. This observation indicates that the packing density of Ncd was higher than accounted for by the model. The model parameters for one-head cooperative binding and the free microtubules are given in Table 2. The parameters include the maximum and minimum radii of the bound motor heads (R_{min} and R_{max}) and the excess scattering cross-section over that of the f_D = 0.42 D_2O solvent (m_0).

Neither the model for binary random one-head binding (Fig. 1*b*) nor that for two-head binding (Fig. 1*c*), the parameters of which are given in Table 2, could be fitted to the data. Random binding (Fig. 1*b*) shows that the very low Q-domain intensity for the model was too low by more than an order of magnitude and the model predicts a second-order peak around Q = 0.042 Å^{-1} that was significantly larger than the observed intensity. These features were a consequence of strong fluctuations of scattering-length density along the microtubules that are present in this case but not in the cooperative-binding case. Two-head binding (Fig. 1*c*) did not accurately give the position of the first-order peak. Attempts to determine whether mixtures of one-head and two-head cooperative binding would improve the overall fit to the data proved futile. However, the inclusion of a small amount of two-head random binding covering 10% of the undecorated microtubule in the one-head cooperative-binding model could explain the relatively broad first-order peak in the data.

It is notable that most of the Ncd construct was not bound to the microtubule. Presumably, all of the motor that passed through the glycerol cushion was bound to the microtubule, decorating 65% of the microtubules, and then re-equilibrated. An estimate of the dissociation constant of the motor head–microtubule complex, $K_D \simeq 25\ \mu M$, was calculated from the data in Tables 1 and 2. This value was larger than the values for microtubule complexes with the dimeric construct MCL (Leu209–Lys700) in the presence of ATP or ATP analogues at 1–1.5 μ*M* in 25 m*M* NaCl (Pechatnikova & Taylor, 1999). The differences may be a consequence of the effect of ionic strength on the stability of the complex as noted in that study.

5. Conclusions

One-head cooperative binding provided the best model for SANS data from Ncd-decorated microtubules. No combination of one-head and two-head binding was consistent with the data. Thus, the solution data are consistent with the AMPPNP-bound state determined by electron microscopy. However, we find that a large fraction of the motors are not bound, suggesting that the complex is not very stable in 100 m*M* NaCl. These results on the states of Ncd may reflect details of its motive mechanism and the results and interpretation of other studies of the complex in solution.

A University of California Directed Research and Development Grant supported part of this work. This work benefited from the use of the Low-Q Diffractometer, LQD, at the Manuel Lujan Jr Neutron Scattering Center of the Los Alamos National Laboratory supported by the US Department of Energy at Los Alamos National Laboratory operated by the University of California under contract No. W-7405-ENG-36 and subsequently by Los Alamos National Security LLC under contract No. DE-AC52-06NA25396. We thank Dr Elena Sablin, UCSF, for providing the Protein Data Bank file containing the coordinates of the Ncd281-decorated tubulin dimer, the laboratory of Dr Roger Cooke, UCSF, for providing the tubulin and Ms Galina Malanina, UCSF, for excellent biochemical assistance.

References

Allingham, J. S., Sproul, L. R., Rayment, I. & Gilbert, S. P. (2007). *Cell*, **128**, 1161–1172.
Andreu, J. M., Bordas, J., Diaz, J. F., Garcia de Ancos, J., Gil, R., Medrano, F. J., Nogales, E., Pantos, E. & Towns-Andrews, E. (1992). *J. Mol. Biol.* **226**, 169–184.
Bracewell, R. N. (1978). *The Fourier Transform and its Applications*, 2nd ed. New York: McGraw–Hill.
Diaz, J. F., Valpuesta, J. M., Chacon, P., Diakun, G. & Andreu, J. M. (1998). *J. Biol. Chem.* **273**, 33803–33810.
Endres, N. F., Yoshioka, C., Milligan, R. A. & Vale, R. D. (2006). *Nature (London)*, **439**, 875–878.
Fink, G., Hajdo, L., Skowronek, K. J., Reuther, C., Kasprzak, A. A. & Diez, S. (2009). *Nature Cell Biol.* **11**, 717–724.

Fletterick, R. J. & Mendelson, R. A. (2010). In preparation.
Foster, K. A. & Gilbert, S. P. (2000). *Biochemistry*, **39**, 1784–1791.
Fujiwara, S., Kull, F. J., Sablin, E. P., Stone, D. B. & Mendelson, R. A. (1995). *Biophys. J.* **69**, 1563–1568.
Furuta, K., Edamatasu, M., Maeda, Y. & Toyoshima, Y. Y. (2008). *J. Biol. Chem.* **283**, 36465–36473.
Furuta, K. & Toyoshima, Y. Y. (2008). *Curr. Biol.* **18**, 152–157.
Gill, S. C. & von Hippel, P. H. (1989). *Anal. Biochem.* **182**, 319–326.
Hjelm, R. P. (1985). *J. Appl. Cryst.* **18**, 452–460.
Hjelm, R. P. (1988). *J. Appl. Cryst.* **21**, 618–628.
Jacrot, B. & Zaccai, G. (1981). *Biopolymers*, **20**, 2413–2426.
Kikkawa, M., Sablin, E. P., Okada, Y., Yahima, H., Fletterick, R. J. & Hirokawa, N. (2001). *Nature (London)*, **411**, 439–448.
Marx, A., Thormahlen, M., Müller, J., Sack, S., Mandelkov, E.-M. & Mandelkov, E. (1998). *Eur. Biophys. J.* **27**, 455–465.
Nogales, E., Wolf, E. G. & Downing, K. H. (1998). *Nature (London)*, **391**, 199–203.
Pechatnikova, E. & Taylor, E. W. (1999). *Biophys. J.* **77**, 1003–1016.
Pettersen, E. F., Goddard, T. D., Huang, C. C., Couch, G. S., Greenblatt, D. M., Meng, E. C. & Ferrin, T. E. (2004). *J. Comput. Chem.* **25**, 1605–1612.
Sablin, E. P. (2000). *Curr. Opin. Cell Biol.* **12**, 35–41.
Sablin, E. P., Case, R. B., Dai, S. C., Hart, C. L., Ruby, A., Vale, R. D. & Fletterick, R. J. (1998). *Nature (London)*, **395**, 813–816.
Sablin, E. P. & Fletterick, R. J. (2004). *J. Biol. Chem.* **279**, 15707–15710.
Seeger, P. A. & Hjelm, R. P. (1991). *J. Appl. Cryst.* **24**, 467–478.
Stone, D. B., Hjelm, R. P. & Mendelson, R. A. (1999). *Biochemistry*, **38**, 4938–4947.
Stone, D. B., Timmins, P. A., Schneider, D. K., Krylova, I., Ramos, C. H. I., Reinach, F. C. & Mendelson, R. A. (1998). *J. Mol. Biol.* **281**, 689–704.
Vale, R. D. (2003). *Cell*, **112**, 467–480.
Vilfan, A., Frey, E., Schwabl, F., Thormählen, M., Song, Y.-H. & Mandelkow, E. (2001). *J. Mol. Biol.* **312**, 1011–1026.
Wendt, T. G., Volkmann, N., Skiniotis, G., Goldie, K. N., Müller, J., Mandelcov, E. & Hoenger, A. (2002). *EMBO J.* **21**, 5969–5978.
White, H. D. (1982). *Methods Enzymol.* **85**, 698–708.
Yun, M., Bronner, C. E., Park, H.-W. & Endow, S. A. (2003). *EMBO J.* **22**, 5382–5389.